

Direct methane operation of a micro-tubular solid oxide fuel cell with a porous zirconia support

Dhruba Panthi¹ · Bokkyu Choi¹ · Atsushi Tsutsumi¹

Received: 7 June 2016 / Revised: 9 August 2016 / Accepted: 11 August 2016 / Published online: 24 August 2016
© Springer-Verlag Berlin Heidelberg 2016

Abstract A novel micro-tubular solid oxide fuel cell (SOFC) design with an inert support was proposed for operation on direct hydrocarbon fuels with an improved stability. In this design, the inert support also serves as a diffusion barrier between the fuel stream and Ni cermet anode. The barrier effect leads to higher local steam to carbon ratios in the anode, thus inhibiting carbon deposition. To demonstrate this concept, we fabricated micro-tubular SOFCs with a porous yttria-stabilized zirconia (YSZ) support. Ni, Ni-scandia-stabilized zirconia (ScSZ), ScSZ, strontium-doped lanthanum manganite (LSM)–ScSZ, and LSM were used as the anode current collector, anode, electrolyte, cathode, and cathode current collector, respectively. Good electrochemical performance was achieved with hydrogen and methane fuels in a temperature range 600–750 °C. Continuous cell operation on direct methane fuel for >40 h at 750 °C under moderate current densities delivered stable voltage without any evident performance degradation due to carbon deposition. The absence of carbon deposition on the anode and anode current collector layers was also confirmed by scanning electron microscope images and energy-dispersive X-ray spectra. We further discuss oxidation mechanism of the direct methane fuel and removal of the carbon possibly formed in the anodic layers during stability testing.

Keywords Micro-tubular SOFC · Inert support · Direct methane operation · Diffusion barrier · Ni-ScSZ anode · Stability

Introduction

In the context of growing demand for energy and environmental concerns related to the use of conventional fossil fuels, significant attention has been paid toward the development of clean energy technologies with high efficiency and low emissions. Fuel cells, which produce electricity directly from hydrogen or hydrogen-rich fuels without intermediate conversions to thermal and mechanical energies, show promise to be a leading technology for the realization of future sustainable energy systems [1, 2]. Solid oxide fuel cells (SOFCs), a class of high-temperature fuel cells with solid ceramic components, offer greater flexibility since they can be operated with a variety of fuels and show low sensitivity to impurities in practical fuels [3, 4]. These fuel cells have a wide range of operating temperature (500–900 °C) and the specific operating temperature can be selected depending on the intended application. Because of their high-temperature exhaust heat, SOFCs are suitable for combined cycle and cogeneration applications, which significantly boost the overall system efficiency [5–8]. An additional advantage of SOFCs is their flexibility in cell and stack designs with different kinds of cell supports and geometric configurations [9].

Owing to the multi-fuel ability of SOFCs, various attempts have been made to operate them with common hydrocarbon fuels such as methane, propane, gasoline, methanol, and ethanol [10–15]. State-of-the-art SOFC anodes containing Ni possess good catalytic properties for the oxidation of hydrocarbon fuels. However, Ni also has a high catalytic activity for

✉ Atsushi Tsutsumi
a-tsu2mi@iis.u-tokyo.ac.jp

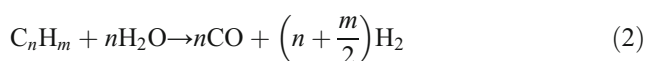
¹ Collaborative Research Center for Energy Engineering, Institute of Industrial Science, The University of Tokyo, 4-6-1 Komaba, Meguro-ku, Tokyo 153-8505, Japan

the cracking of the hydrocarbon compounds at high temperatures, as given by the following reaction.



The catalytic cracking of the fuel causes carbon deposition on the anode, usually involving growth of carbon nanofibers, and this leads to severe degradation in anode performance because of the loss of active reaction sites, restriction to gas flow, and microstructure damage [16–18].

In conventional SOFC systems fueled with hydrocarbons, steam is generally fed together so as to achieve internal reforming of the hydrocarbons and prevent their cracking.



Since Reaction 2 is an endothermic reaction, internal reforming SOFC systems are expected to improve SOFC power generation efficiency by optimally utilizing the high-temperature heat released by exothermic fuel cell reactions. However, there are two main practical problems associated with internal reforming: (i) a high steam to carbon (S/C) ratio (>2) is required to fully suppress carbon formation, which decreases the Nernst potential of the cell and also adds cost and complexity to the system, and (ii) highly endothermic nature of the steam reforming reaction results in an uneven temperature distribution across the cell including the formation of “cold spots” [19].

As an alternative approach to reforming, several researchers have put their efforts to achieve direct oxidation of dry or slightly humidified hydrocarbon fuels at the SOFC anode by preventing carbon deposition [20, 21]. One of the strategies for this has been to use alternative anode materials that do not promote carbon deposition. Although considerable improvements have been made to the performance of alternative anode materials containing Cu or conductive perovskites such as (La,Sr)(Cr,Mn)O₃ and doped SrTiO₃, Ni cermet is still a preferred anode material owing to its superior electronic conductivity as well as electrocatalytic properties [22]. Therefore, attempts have been made to utilize direct hydrocarbon fuels in SOFCs by modifying the Ni cermet anodes. Surface modification and alloying of Ni cermets with carbon-resistant metals and oxides, such as Cu [23], Sn [24], Ag [25], and CeO₂ [26], were found to be effective for suppressing carbon deposition. Additionally, stable cell operations could be achieved by identifying suitable operating conditions such as temperature, current density, and fuel composition, at which carbon coking and consequent anode degradation can be minimized. For example, Lin et al. [27] studied the operation of Ni–yttria-stabilized zirconia (YSZ) anode supported SOFCs on methane fuel in detail and demonstrated

that stable operations without carbon coking were possible at $T \leq 700$ °C under moderate current densities. It was considered that the reaction products of the electrochemical oxidation of methane (H₂O and CO₂) helped suppress carbon build-up in the anode.

Recently, a concept of using a diffusion barrier between the fuel stream and anode was introduced to improve the stability of Ni cermet SOFC anodes fueled with direct hydrocarbons [28–30]. A schematic representation of the variation in concentration of fuel and product gases from the fuel stream to the anode–electrolyte interface during SOFC operation for anode-supported designs without and with the barrier layer is shown in Fig. 1(a, b), respectively. The diffusion barrier made of an inert ceramic material results in decreased fuel content and increased product content toward the anode. This increases local S/C ratios in the anode, and thus, suppresses carbon deposition. Stable operations on direct methane fuel were achieved at temperatures up to 800 °C under practical current densities by applying an inert barrier layer containing partially stabilized zirconia and CeO₂ to a Ni–YSZ anode supported button cell [28]. Rosensteel et al. [31] also demonstrated a stable operation of a Ni–YSZ supported tubular SOFC on simulated biogas fuel using a chemically inert, porous ceramic barrier. Although the barrier layer technology has successfully been applied to planar and large tubular SOFCs, it has not been studied so far for micro-tubular SOFCs which have typical diameters ≤ 5 mm and offer several advantages such as facile sealing, high volumetric power density, and better resistance to thermal cycling and thermal shock.

In our previous studies, we proposed a novel micro-tubular SOFC design with an inert support and an integrated current collecting layer for the inner electrode to improve current collection efficiency and reduction–oxidation (redox) stability of the cell [32–35]. Since the inert support itself serves as a diffusion barrier to the Ni cermet anode as illustrated in Fig. 1(c), this micro-tubular SOFC is expected to run stably on direct hydrocarbon fuels. It is notable that because of the thick inert support and thin Ni-containing anodic layers (anode current collector and anode), concentration ratio of the product gases to the hydrocarbon fuel along the surface AA', where carbon deposition is most likely, will be highest for the inert support-based design (Fig. 1a–c). This could further reduce the possibility of carbon deposition on the anodic layers. In the present work, we demonstrated the effectiveness of the inert support as a diffusion barrier for direct methane operations by fabricating micro-tubular SOFCs using porous YSZ as the inert support. The electrochemical performance of the fabricated cells was evaluated with hydrogen and methane as the fuels. The stability of cell operation on direct methane fuel was then examined by monitoring the cell voltage at moderate current densities for an extended period.

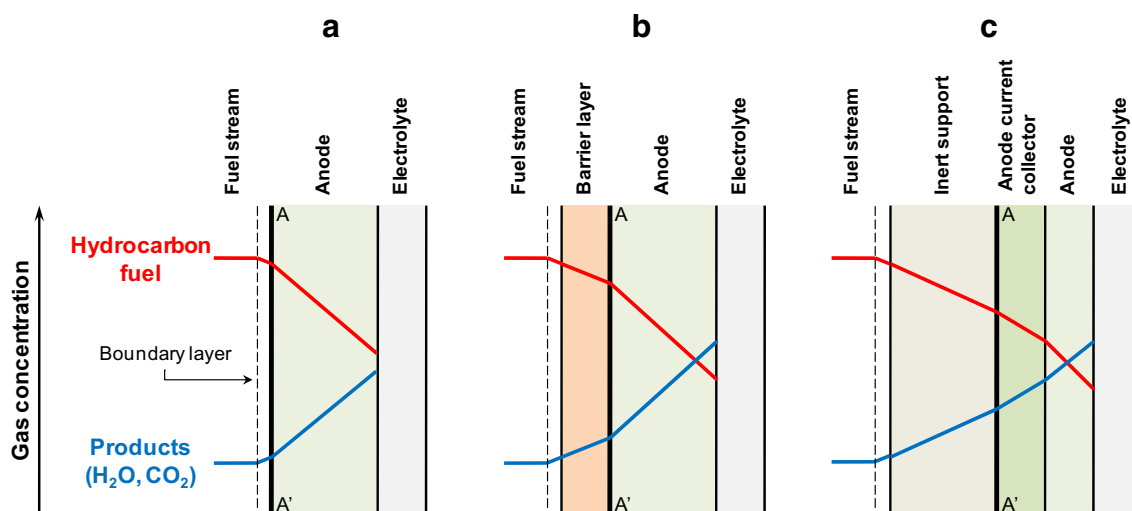


Fig. 1 Schematic of the variation in concentration of fuel and product gases from fuel stream to anode-electrolyte interface during SOFC operation for different cell designs: **a** conventional anode-supported design, **b** anode-supported design with a barrier layer, and **c** inert

support-based design. AA' represents a surface where the fuel first comes into contact with Ni-containing anode (or anode current collector) and carbon deposition is most likely

Experimental

The micro-tubular SOFC samples were prepared by multi-step dip coating and cosintering methods [36]. YSZ, Ni, Ni-scandia-stabilized zirconia (ScSZ), ScSZ, strontium-doped lanthanum manganite (LSM)-ScSZ, and LSM were used as the inert support, anode current collector, anode, electrolyte, cathode, and cathode current collector, respectively, as shown schematically in Fig. 2. The details of the materials used for the different cell components are given in Table 1. To impart desired porosity to the YSZ support, 10 wt% micro-crystalline cellulose (Avicel, Merck, Germany) and 10 wt% polymethyl methacrylate (PMMA; 2.9 μm , Soken, Japan) were used as pore formers. Similarly, 10 wt% micro-crystalline cellulose (20 μm , Sigma Aldrich, USA) was used as a pore former for the NiO anode current collector. A mixture of ethanol and toluene was used as a solvent to prepare the respective slurries. To achieve desired slurry properties, calculated amounts of polyvinyl butyral (Butvar B-98, Sigma Aldrich), tallow propylene diamine (Diamin RRT, Kao, Japan), and dioctyl phthalate (Sigma Aldrich) were added as a binder, dispersant, and plasticizer. A further description of the cell fabrication process can be found in our previous papers [34, 35]. With a mean electrolyte diameter of 3.6 mm and active (cathode) length of 8 mm, the fabricated cell had an active surface area of 0.9 cm^2 .

To evaluate the electrochemical performance, the SOFC sample was connected to a fuel supply tube inside an electric furnace, as illustrated in Fig. 3. Alumina cement (Ceramabond 552, Aremco, USA) was used as a high-temperature gas seal. Platinum wires were used as current and voltage leads, and they were attached to the electrode surfaces with platinum paste. The electrochemical measurements were carried out

with a potentiostat (1480 Multistat, Solartron, UK) combined with a frequency response analyzer (1255B, Solartron). Methane or hydrogen humidified with 3 vol% water was fed to the anode at a flow rate of 20 mL min^{-1} , whereas ambient air was fed to the cathode at a flow rate of 20,000 mL min^{-1} . It is to be noted that the air flow rate was relatively high because of a large furnace size (internal diameter = 200 mm). The electrochemical impedance spectroscopy (EIS) data were obtained in a frequency range from 100 kHz to 100 mHz by applying an AC perturbation of 10 mV and a DC load of 400 mA cm^{-2} . The DC load was applied in order to avoid carbon deposition on the anode and anode current collector layers when using methane as the fuel. To check cell stability under direct methane operation, the cell was subjected to a constant load current of 500 mA cm^{-2} and its voltage was monitored for an extended period. Further stability tests

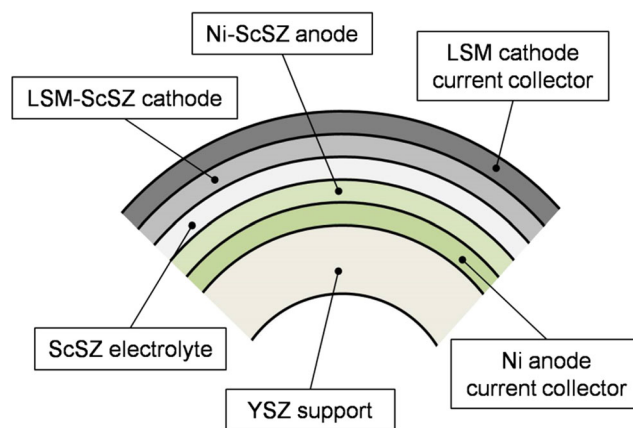


Fig. 2 Schematic cross-section of the micro-tubular SOFC with a porous YSZ support

Table 1 Materials used for the fabrication of micro-tubular SOFC samples

Cell component	Material	Supplier
Support	YSZ (TZ-8Y)	Tosoh, Japan
Anode current collector	NiO (NiO-AS)	Kceracell, South Korea
Anode	60 wt% NiO (NiO-AFL) 40 wt% ScSZ (10Sc1CeSZ)	Kceracell Daiichi Kigenso, Japan
Electrolyte	ScSZ (10Sc1CeSZ)	Daiichi Kigenso
Cathode	50 wt% LSM (LSM-80F) 50 wt% ScSZ (10Sc1CeSZ)	Daiichi Kigenso Daiichi Kigenso
Cathode current collector	LSM (LSM-80F)	Daiichi Kigenso

were also conducted at lower current densities for shorter periods. A scanning electron microscope (SEM; JSM-7000F, JEOL, Japan) equipped with an energy dispersive X-ray (EDX) unit was used to examine the cell microstructure before and after the electrochemical tests. The open porosity of the YSZ support was determined using an Archimedes' method with deionized water as the immersion medium.

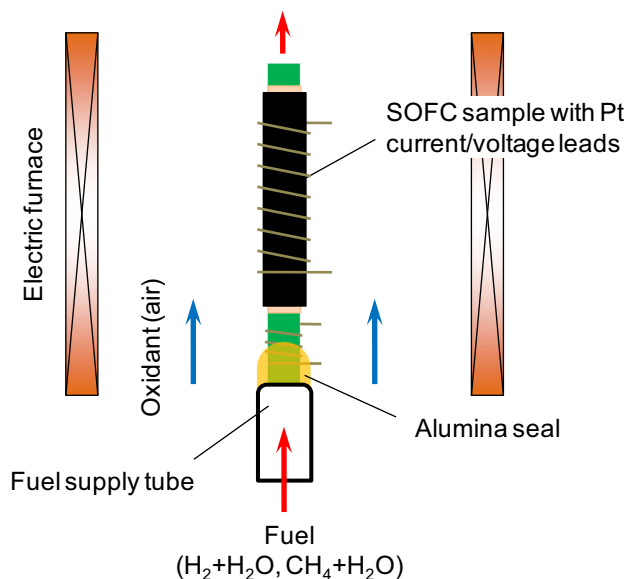
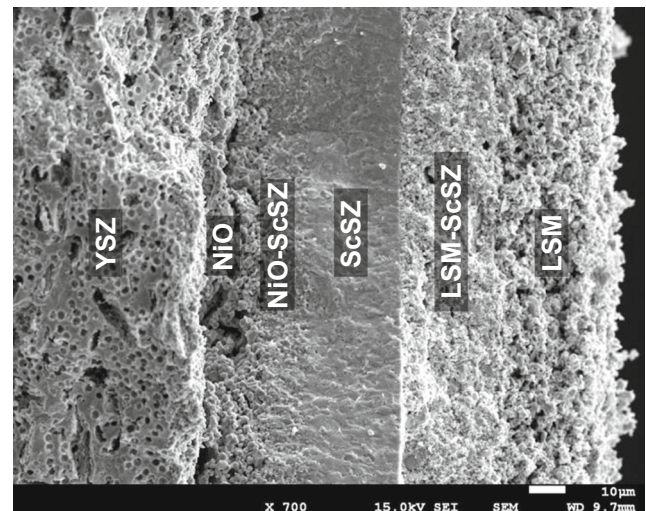
Results and discussion

A cross-sectional microstructure of the as-prepared micro-tubular SOFC is shown in Fig. 4. The approximate thicknesses of the anode current collector, anode, electrolyte, cathode, and cathode current collector layers were 17, 12, 27, 29, and 28 μm , respectively. There was a good adherence between the adjacent cell layers. The electrolyte layer was dense and free of micro-cracks or pinholes. The open porosity of the YSZ support was determined to be $\sim 43\%$. This porosity was found to be close to an optimum value considering gas

transport to the anode and mechanical strength of the cell [34, 35].

The I - V characteristic curves obtained from single cell tests with hydrogen and methane as the fuels are shown in Fig. 5(a, b), respectively. With the hydrogen fuel, the cell yielded maximum power densities of 724, 592, 468, and 346 mW cm^{-2} at 750, 700, 650, and 600 $^{\circ}\text{C}$, respectively. When the fuel was switched from hydrogen to methane, the maximum power densities of 524, 346, 192, and 96 mW cm^{-2} were obtained at 750, 700, 650, and 600 $^{\circ}\text{C}$, respectively. These power densities for hydrogen and methane operations are comparable with those reported in the literature [27, 37]. The decrease in the power density of the cell with methane is attributed to slower electrochemical oxidation of methane than that of hydrogen in the Ni-ScSZ anode. Additionally, it is notable that the catalytic activity of Ni-based anodes for methane oxidation decreases sharply at lower temperatures [38]. Therefore, the difference between the power densities for hydrogen and methane was more pronounced with the decreasing operating temperature.

To determine different resistances associated with cell operations on hydrogen and methane fuels, impedance

**Fig. 3** Schematic of the experimental setup for electrochemical measurements**Fig. 4** Cross-sectional SEM micrograph of a typical SOFC sample before electrochemical testing

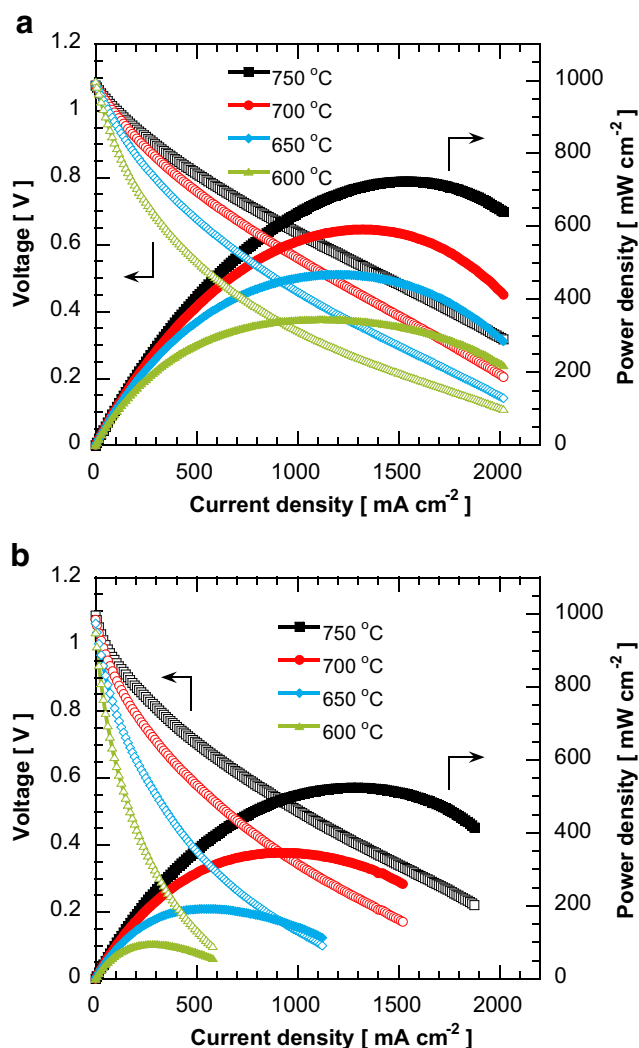


Fig. 5 *I*-*V* Characteristic curves for single cell operation on **a** hydrogen and **b** methane

measurements were conducted. Figure 6(a) shows impedance spectra for the single cell at 750 °C. A simple equivalent circuit, as shown in Fig. 6(b), was used to fit these impedance spectra. The different cell resistances obtained from the fitted data for hydrogen and methane operations are given in Table 2. As can be seen, the total cell resistance (R_{Total}) was dominated by R_{Ohm} and R_1 . R_{Ohm} was slightly larger for the methane operation and this is likely due to reduction in local cell temperature caused by endothermic reforming reactions, which led to a lower ionic conductivity of the electrolyte [31]. The high-frequency resistance (R_1) for methane was clearly larger than that for hydrogen, whereas there was not much difference between the low-frequency resistances (R_2). The high-frequency resistance is considered to be associated with fuel oxidation reaction at the anode, and the low-frequency resistance is attributed to oxygen reduction reaction at the cathode and gas diffusion losses [27, 39]. Thus, higher activation polarization for fuel oxidation reaction at the anode was

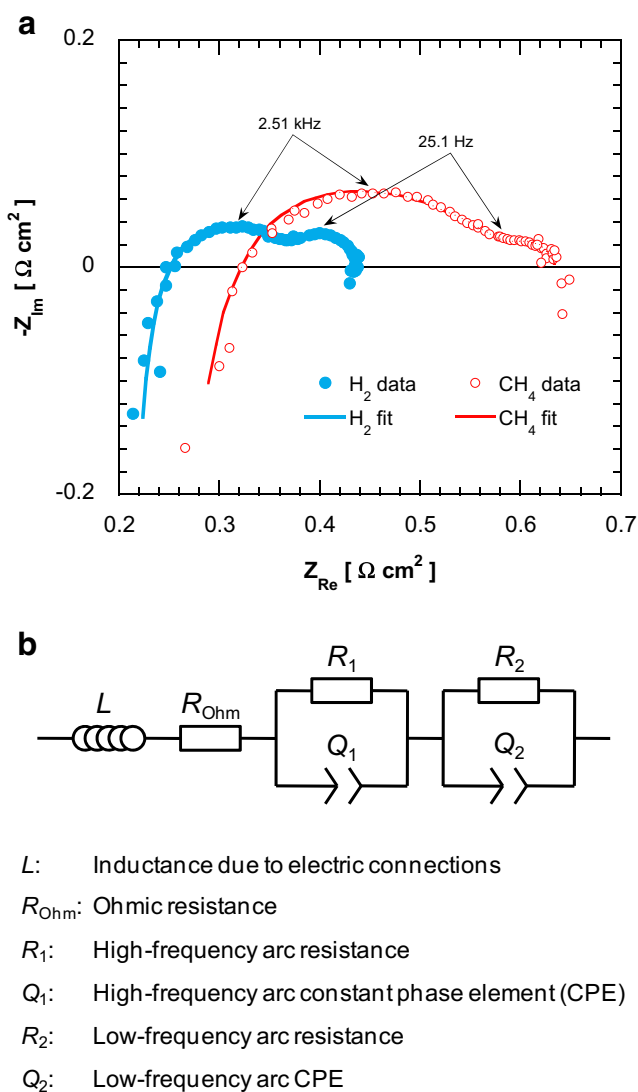


Fig. 6 **a** Impedance spectra for single cell at 750 °C under a load current of 400 mA cm⁻². **b** Equivalent circuit model used to fit the impedance data

primarily responsible for higher total cell resistance and hence lower power densities with the methane fuel. This is also indicated by the higher slope of the *I*-*V* curves for methane at small current densities, i.e. in the activation region.

Figure 7(a) shows a plot of voltage versus time for cell operation on the methane fuel at 750 °C under a load current of 500 mA cm⁻². The initial voltage was recorded to be ~0.72 V. Although this voltage decreased slightly to ~0.70 V

Table 2 Comparison of area-specific resistances for H₂ and CH₄ operations

	R_{Ohm}	R_1	R_2	R_{Total}
H ₂	0.20	0.19	0.05	0.44
CH ₄	0.22	0.39	0.03	0.64

All resistance values are given in Ω cm²

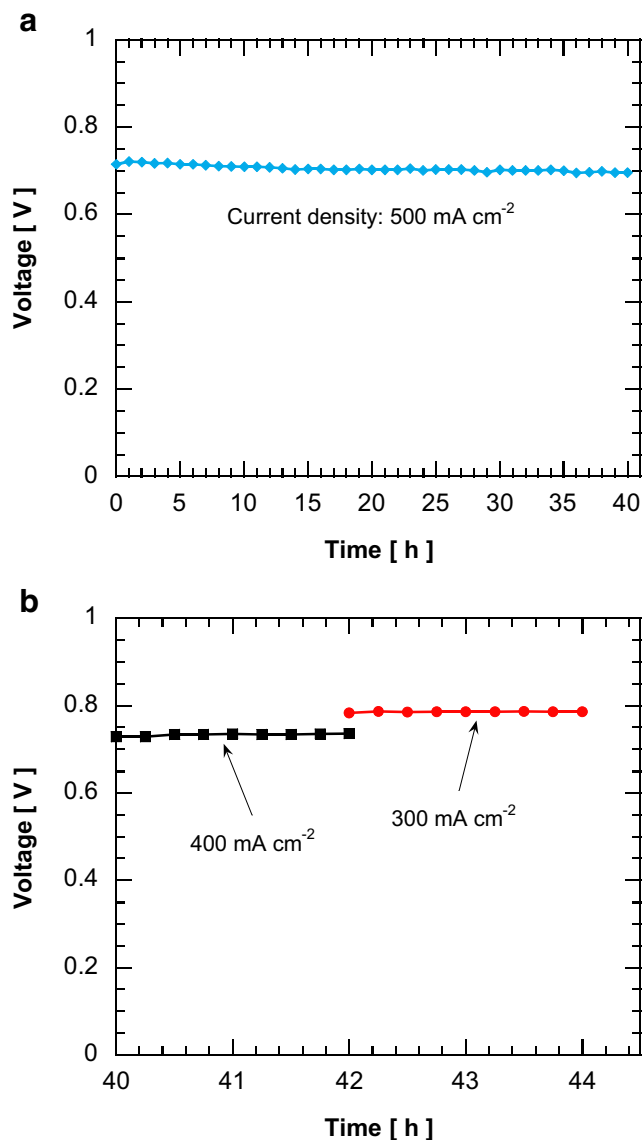


Fig. 7 Stability testing in methane at 750 °C under different load currents: **a** 500, **b** 400, and 300 mA cm⁻²

after 40 h operation, the cell showed good stability in methane without any evident performance degradation due to carbon deposition. To further check the stability of the cell at lower current densities, the load current was decreased first to 400 and then to 300 mA cm⁻², and the cell was operated for 2 h under each load current, as shown in Fig. 7(b). The cell still exhibited a stable performance with nearly constant voltages of 0.73 and 0.79 V at 400 and 300 mA cm⁻², respectively. To check if there was any carbon deposition on the anode and/or anode current collector layers after stability testing, SEM and EDX characterizations were conducted. Cross-sectional microstructure of the sample subjected to stability testing is shown in Fig. 8(a). As shown by the magnified views of the anode and anode current collector layers, no carbon deposition was observed. The absence of carbon deposition was further

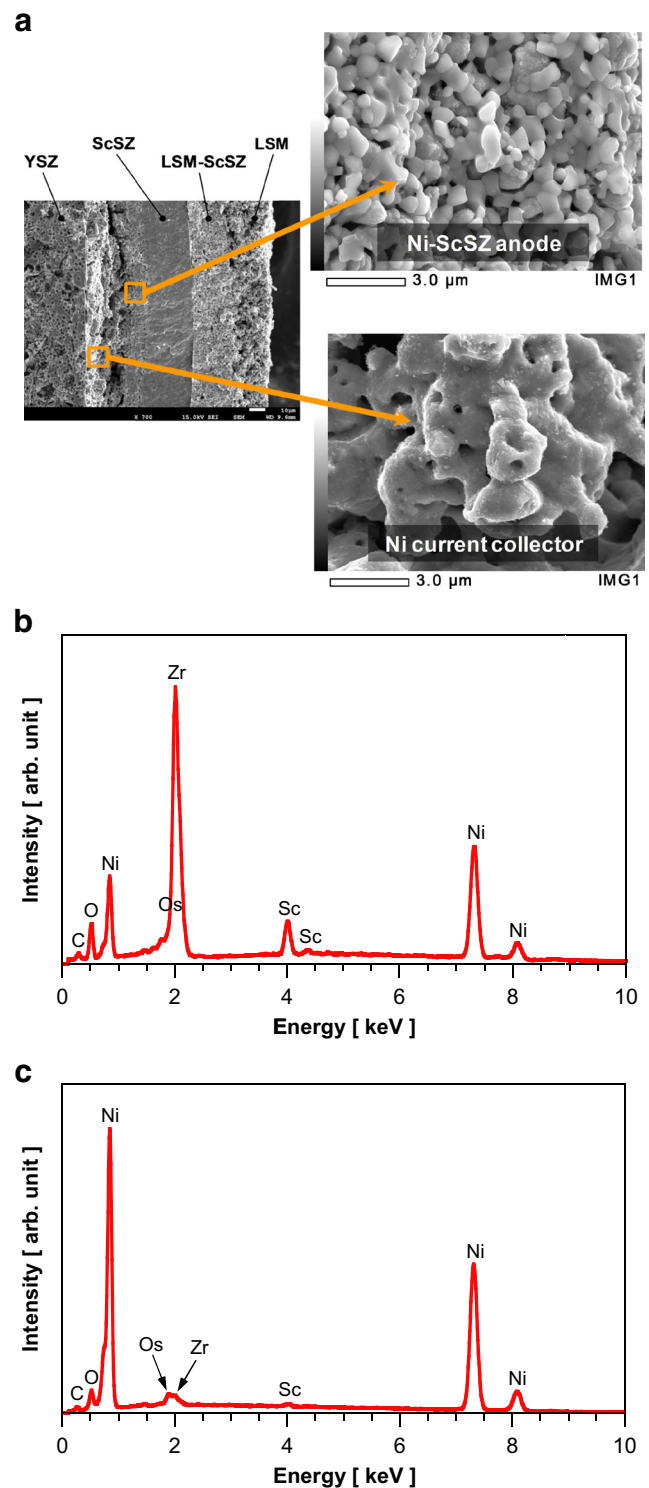


Fig. 8 Microstructure characterization after stability testing: **a** SEM micrograph of the cell cross-section with magnified views of anode and anode current collector, **b** EDX spectra for anode cross-section, and **c** EDX spectra for anode current collector cross-section. Note that Os peaks were resulted from a conductive Os coating applied to the sample before SEM/EDX observation

confirmed by EDX spectra obtained from the anode and anode current collector layers, as shown in Fig. 8(b, c), respectively.

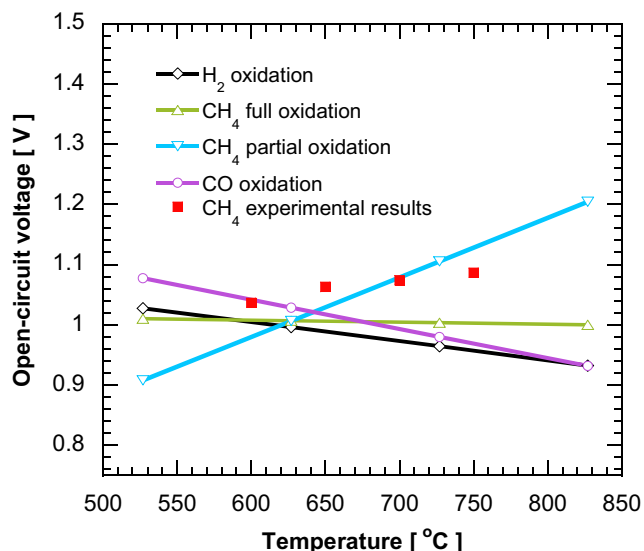
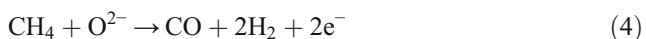
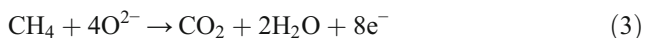


Fig. 9 Comparison of theoretical OCVs for different oxidation reactions and experimental values obtained with methane. For all OCV calculations, ambient air was considered as the oxidant

Both the layers had very small peaks for C, suggesting that there was no carbon build-up due to methane cracking. For comparison, it is notable that the Ni–zirconia anodes with clear carbon deposition result in EDX spectra with C peaks as strong as Zr peaks [40].

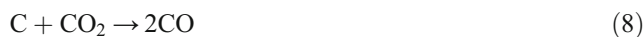
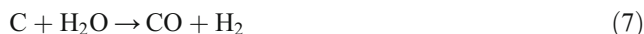
To describe oxidation mechanism of the direct methane fuel in the present study, theoretical open-circuit voltages (OCVs) for possible electrochemical oxidation reactions were calculated and plotted against temperature, as shown in Fig. 9. From a thermodynamic point of view, the anode of a methane-fueled SOFC may contain a maximum of six species formed by the decomposition and/or reforming reactions at high temperatures: CO, H₂, CO₂, H₂O, C, and residual CH₄ [22]. Among these species, CH₄, CO, and H₂ may be oxidized by the electrochemically pumped oxygen ions. Thus, the main possible electrochemical oxidation reactions are considered to be methane full oxidation (Reaction 3), methane partial oxidation (Reaction 4), hydrogen oxidation (Reaction 5), and carbon monoxide oxidation (Reaction 6) [22, 41].



The OCV for the methane full oxidation reaction does not vary much with the operating temperature, whereas that for the methane partial oxidation reaction increases distinctly when the temperature is increased. On the other hand, the OCVs for the hydrogen and carbon monoxide oxidation

reactions decrease with an increase in the temperature. As also plotted in Fig. 9, the experimental results for methane showed an increasing trend of the OCV with the operating temperature. Thus, the dominant oxidation reaction is likely the methane partial oxidation reaction. Previous studies for direct methane operations have also reported that the methane partial oxidation dominates the overall reaction [27, 41]. Despite the dominance of methane partial oxidation, other oxidation reactions may also take place simultaneously. For example, some of the methane fuel may undergo full oxidation reaction while the product gases of partial oxidation (H₂ and CO) may further be oxidized to H₂O and CO₂.

From the stability test results, it is apparent that the carbon build-up in the anode and anode current collector layers was inhibited owing to the presence of the product gases (steam and carbon dioxide) in these layers. Because of the barrier effect of the inert support, there was a lower concentration of methane and higher concentration of steam and carbon dioxide in the anode, thus leading to a less favorable condition for carbon deposition. As discussed above, the possible electrochemical routes for the production of steam and carbon dioxide include methane full oxidation (Reaction 3), and oxidation of hydrogen and carbon monoxide (Reactions 5 and 6) formed by the partial oxidation of methane. Although some solid carbon may have been formed during cell operation for extended hours, it was removed probably through the following reactions and cell degradation due to carbon deposition was prevented [27].



Conclusions

We examined the stability of a novel micro-tubular SOFC with an inert support for operation on direct methane fuel. The micro-tubular SOFC samples fabricated in this study contained YSZ, Ni, Ni-ScSZ, ScSZ, LSM-ScSZ, and LSM as the inert support, anode current collector, anode, electrolyte, cathode, and cathode current collector, respectively. The cell showed good electrochemical performance with both hydrogen and methane fuels. As a result of the barrier effect of the inert support, stable cell operation was achieved with the direct methane fuel under a current density as low as 300 mA cm⁻² at 750 °C. SEM/EDX observation of the sample subjected to stability testing showed that there was no carbon build-up due to methane cracking in the anode and anode current collector layers. By comparing the experimental and theoretical OCV values, partial oxidation of methane was speculated to be the dominant oxidation reaction in the anode. It is likely that any solid carbon formed in the anode and anode

current collector layers during cell operation for extended hours was removed by reaction with product species (steam and carbon dioxide) in these layers. Our results indicate that the inert support-based micro-tubular SOFC presented here is suitable for stable operation on direct hydrocarbon fuels with a wide operating window. In addition, this micro-tubular SOFC is expected to provide a better stability under redox conditions and improved current collection through the Ni current collector, as suggested by our previous studies.

Acknowledgments This work was supported by JSPS KAKENHI (Grant Number 15H04250).

References

1. Steele BCH, Heinzel A (2001) *Nature* 414:345–352
2. Edwards PP, Kuznetsov VL, David WIF, Brandon NP (2008) *Energy Policy* 36:4356–4362
3. Ormerod RM (2003) *Chem Soc Rev* 32:17–28
4. Wachsmann ED, Lee KT (2011) *Science* 334:935–939
5. Kuchonthara P, Bhattacharya S, Tsutsumi A (2003) *J Power Sources* 124:65–75
6. Kuchonthara P, Bhattacharya S, Tsutsumi A (2005) *Fuel* 84:1019–1021
7. Zhang X, Chan SH, Li G, Ho HK, Li J, Feng Z (2010) *J Power Sources* 195:685–702
8. Buonomano A, Calise F, d'Accadia MD, Palombo A, Vicidomini M (2015) *Appl Energy* 156:32–85
9. Minh NQ (2004) *Solid State Ionics* 174:271–277
10. Murray EP, Tsai T, Barnett SA (1999) *Nature* 400:649–651
11. Park S, Vohs JM, Gorte RJ (2000) *Nature* 404:265–267
12. Sasaki K, Watanabe K, Shiosaki K, Susuki K, Teraoka Y (2004) *J Electroceram* 13:669–675
13. Zhan Z, Barnett SA (2005) *Science* 308:844–847
14. Yang L, Wang S, Blinn K, Liu M, Liu Z, Cheng Z, Liu M (2009) *Science* 326:126–129
15. Ye XF, Yuan C, Chen YP, Zhong CY, Zhan ZL, Wang SR (2014) *J Electrochem Soc* 161:F894–F898
16. Sumi H, Yamaguchi T, Hamamoto K, Suzuki T, Fujishiro Y (2012) *J Power Sources* 220:74–78
17. Kim Y, Kim JH, Bae J, Yoon CW, Nam SW (2012) *J Phys Chem C* 116:13281–13288
18. Miao H, Liu G, Chen T, He C, Peng J, Ye S, Wang WG (2015) *J Solid State Electrochem* 19:639–646
19. Mogensen M, Kammer K (2003) *Annu Rev Mater Res* 33:321–331
20. Atkinson A, Barnett S, Gorte RJ, Irvine JT, McEvoy AJ, Mogensen M, Singhal SC, Vohs J (2004) *Nature Mater* 3:17–27
21. Tsipis EV, Kharton VV (2011) *J Solid State Electrochem* 15:1007–1040
22. Wang W, Su C, Wu Y, Ran R, Shao Z (2013b) *Chem Rev* 113:8104–8151
23. Kim H, Lu C, Worrell WL, Vohs JM, Gorte RJ (2002) *J Electrochem Soc* 149:A247–A250
24. Nikolla E, Schwank J, Linic S (2009) *J Electrochem Soc* 156:B1312–B1316
25. Wu X, Zhou X, Tian Y, Kong X, Zhang J, Zuo W, Ye X, Sun K (2015) *Int J Hydrog Energy* 40:16484–16493
26. Qiao J, Zhang N, Wang Z, Mao Y, Sun K, Yuan Y (2009) *Fuel Cells* 9:729–739
27. Lin Y, Zhan Z, Liu J, Barnett SA (2005) *Solid State Ionics* 176:1827–1835
28. Lin Y, Zhan Z, Barnett SA (2006) *J Power Sources* 158:1313–1316
29. Zhu H, Colclasure AM, Kee RJ, Lin Y, Barnett SA (2006) *J Power Sources* 161:413–419
30. Bierschenk DM, Pillai MR, Lin Y, Barnett SA (2010) *Fuel Cells* 10:1129–1134
31. Rosensteel WA, Babiniec SM, Storzjohann DD, Persky J, Sullivan NP (2012) *J Power Sources* 205:108–113
32. Panthi D, Tsutsumi A (2013) *ECS Trans* 57:789–798
33. Panthi D, Tsutsumi A (2014a) *Sci Rep* 4:5754
34. Panthi D, Choi B, Tsutsumi A (2015a) *Int J Hydrog Energy* 40:10588–10595
35. Panthi D, Choi B, Tsutsumi A (2015b) *J Electrochem Soc* 162:F1555–F1560
36. Panthi D, Tsutsumi A (2014b) *J Solid State Electrochem* 18:1899–1905
37. Huang B, Ye XF, Wang SR, Nie HW, Shi J, Hu Q, Qian JQ, Sun XF, Wen TL (2006) *J Power Sources* 162:1172–1181
38. Wang W, Ran R, Su C, Guo Y, Farrusseng D, Shao Z (2013a) *J Power Sources* 240:232–240
39. Koh JH, Yoo YS, Park JW, Lim HC (2002) *Solid State Ionics* 149:157–166
40. Liu J, Barnett SA (2003) *Solid State Ionics* 158:11–16
41. Kendall K, Finnerty CM, Saunders G, Chung JT (2002) *J Power Sources* 106:323–327